Available online at www.sciencedirect.com
SCIENCE DIRECT
International Journal of Heat and Mass Transfer 49 (2006) 3229–3239
International Journal of HEAT and MASS TRANSFER
www.elsevier.com/locate/ijhmt

Effects of pressure on thermal transport in plutonium oxide powder

Patricia A. Bielenberg [a], F. Coyne Prenger [b], D. Kirk Veirs [a,*], Gerard F. Jones [c]

[a] Nuclear Materials Technology Division, Los Alamos National Laboratory, MS E505, P.O. Box 1663, MS E505, Los Alamos, NM 87545, United States
[b] Engineering Science and Applications Division, Los Alamos National Laboratory, MS J580, P.O. Box 1663, Los Alamos, NM 87545, United States
[c] Department of Mechanical Engineering, Villanova University, 800 Lancaster Ave., Villanova, PA 19085, United States

Received 4 November 2004; received in revised form 26 January 2006
Available online 24 March 2006

Abstract

Radial temperature profiles of plutonium dioxide powder in a cylindrical vessel were measured over a pressure range of 0.055 to 334.4 kPa with two different fill gases, helium and argon. The powder provides a very uniform self-heating medium for analysis. A thermal conductivity model was developed for heat conduction in the fine ceramic powder. Most literature models make limiting assumptions about powder characteristics that do not hold for this material. Despite the powder particles' complex geometry, the proposed model correctly reproduces the powder temperature profiles over the wide pressure range for both fill gases.

Keywords: Thermal conductivity; Plutonium dioxide; Porous; Powder

1. Introduction

The contraction of the nuclear weapons complex has resulted in a significant amount of plutonium material that needs to be stored safely for up to 50 years before final disposition. The relevant Department of Energy (DOE) standard requires that storage containers have a maximum Pu and other fissile species mass of 4.40 kg, a maximum total mass of 5.00 kg, a maximum power generation rate of 19 W, and a maximum moisture content of 0.5 wt.% [1]. For pure weapons-grade plutonium oxide powder, a container can be loaded to its 5.00 kg limit since 5.00 kg plutonium dioxide (PuO_2) contains 4.40 kg Pu. These specifications have been established to ensure safe temperature and pressure limits for the containers while in storage.

One concern for long-term stability of these containers is over-pressurization that could result in accidental release of container contents. The heat generating plutonium oxide powder provides a heat source in the storage container. Pressure increases can occur due to gas generation from radiolysis of residual water in the container, from steam generation of the residual water at high temperatures, and from fill-gas expansion as the temperature increases. Two previous studies have been conducted to estimate temperatures in the plutonium oxide storage containers [2,3]. One severe limitation of these studies was the lack of information concerning the effective thermal conductivity of the PuO_2 packed-powder bed. (Note: the thermal conductivity of the powder, including the gas and PuO_2 solid, will be referred to as the effective thermal conductivity from here on.) In the previous PuO_2 heat transfer studies, the effective thermal conductivity was estimated from a packed bed model, the Deissler–Eian correlation [4]. This correlation estimates the effective thermal conductivity in terms of the porosity and the thermal conductivities of the gas and solid. At the high porosities (60–80%) commonly observed in these powders, this correlation is relatively insensitive to the solid thermal conductivity. Part of the motivation to measure the effective thermal conductivity of the PuO_2 powder in the current study is to assess the effectiveness of this correlation.

* Corresponding author. Tel.: +1 505 667 9291; fax: +1 505 665 4394.
E-mail address: veirs@lanl.gov (D.K. Veirs).

0017-9310/$ - see front matter © 2006 Elsevier Ltd. All rights reserved.
doi:10.1016/j.ijheatmasstransfer.2006.01.027

Nomenclature

A	area (m^2)
B_1	PuO_2 solid conductivity parameter (m K W^{-1})
B_2	PuO_2 solid conductivity parameter (m W^{-1})
C_p	heat capacity (J kg^{-1} K^{-1})
d	gap distance between particles in unit cell (m)
D	length of the unit cell (m)
D_m	molecular diameter (m)
e	emissivity
G	conductance (W K^{-1})
h	heat transfer coefficient (W m^{-2} K^{-1})
l	mean free path (m)
L	length (m)
L/D	interparticle contact fraction
k_B	Boltzmann's constant (J K^{-1})
k	thermal conductivity (W m^{-1} K^{-1})
Kn	Knudsen number
m	mass (kg)
n_{emiss}	radiation cell density (m^{-1})
P	pressure (Pa)
Q	heat flow rate (W)
q	specific heat flow rate (W kg^{-1})
r	radial position (m)
R	radius (m)
T	temperature (K)

Greek symbols

α	thermal accommodation coefficient
δ	contact roughness
ε	porosity
ϕ	sphericity
κ_T	thermal diffusivity (m^2 s^{-1})
λ	pore diameter (m)
Λ_o	free molecular conductivity parameter (W m^{-2} K^{-1} Pa^{-1})
ρ	density (kg m^{-3})
σ	Stefan–Boltzmann constant (W m^{-2} K^{-4})

Subscripts

a	air
ax	axial
b	bed
cont	continuum regime
eff	effective value for powder
expt	experimentally measured
ext	external surface of the container
fm	free molecular
g	gas
gen	generation
i	radial node in model
in	interparticle region in unit cell
j	axial node in model
nrad	number of radial nodes in model
nax	number of axial nodes in model
o	outer "gas" region
out	outer edge of radial node in model
PuO_2	plutonium oxide
r	radial
ref	reference
s	"solid" component of the powder
solid	solid particle
trans	transition pressure region
w	wall

Models in the literature to calculate effective thermal conductivities of packed beds have been reviewed previously [5–7]. The simpler correlations, such as the Deissler–Eian model or Maxwell's model, require the bed porosity and the thermal conductivities of the solid and the gas. More complex models often contain many parameters to capture factors like particle size, shape, dispersity, and packing. Plutonium oxide powders are typically very fine powders with high porosity and randomly shaped particles [8]. For these powders, most of these parameters can only be estimated by comparison with results from experimental data; they cannot be easily estimated *a priori*. Thus, the unknown characteristics of the PuO_2 bed precludes our use of the more complex packed bed thermal conductivity models.

In this paper, an experimental and modeling study of heat transfer in PuO_2 powder beds to improve understanding of thermal transport in these powders will be presented. Radial temperature profiles in PuO_2 powder in the storage containers were measured at varying pressures with two different fill gases to determine the thermal behavior of the powder over a wide range of conditions. A mechanistic thermal model incorporating the multiple thermal pathways present was developed to aid in the analysis of the experimental data and to provide predictive capabilities. The effective thermal conductivity of these powder beds is calculated based on the bed porosity, pore size, interstitial gas pressure, and the thermal conductivities of the interstitial gas and 100% dense solid. The proposed thermal model provides a more accurate prediction of heat transfer rates in the PuO_2 powder in the storage containers than do correlations from previous studies.

2. Experimental measurements

Radial temperature profile measurements were performed on a PuO_2 powder bed in a cylindrical stainless steel (SS316) container. The PuO_2 powder provided a constant volumetric heat source in which to measure steady-state temperature profiles. The container dimensions were 21.4 cm high with a 5.7 cm radius in accordance with the dimensions of a DOE approved storage container system,

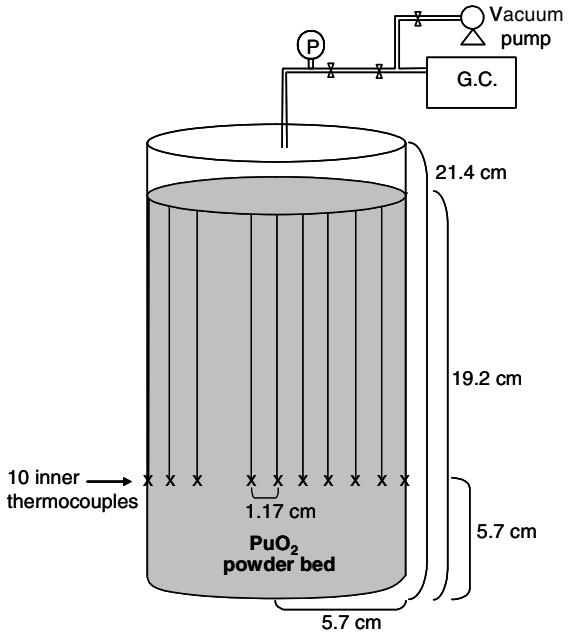

Fig. 1. Schematic of the experimental apparatus. Additional thermocouples were located on the outside of the container wall and in the surrounding air.

shown in Fig. 1. The bed height was 19.2 cm and temperature measurements were made from 10 thermocouples located radially across the container at a height of 5.7 cm along with additional thermocouples on the outside of the container.

The bodies of the sheathed Type E thermocouples (Omega EMQSS-020) were aligned axially within the bed and extended to the top of the bed to minimize temperature perturbations at the point of measurement. The thermocouples were interfaced to a National Instruments SCXI 1303 terminal block for high-accuracy thermocouple measurements that input to a National Instruments SCXI 1102 32-channel analog and thermocouple input module. The input module was read using a National Instrument E Series multifunction data acquisition board by a LabView program. Data were stored every 15 min. The thermocouple terminal block/input module/DAC electronics were calibrated using an Omega CL25 high precision handheld calibrator. When the calibrator was inserted at the thermocouple connector immediately outside the container, the computer data agreed with the calibrator over the range of 298.2 K to 673.2 K to 0.1 K, which was the precision of the calibrator read-out. The thermocouples as received from Omega have a reported absolute accuracy of 1.7 K. Ambient temperature readings for all thermocouples prior to loading the container with the plutonium oxide powder agreed with each other to 0.1 K. Since the thermocouples all agree with each other, the relative temperature difference measurements will have higher accuracy than the reported absolute accuracy of 1.7 K.

The system pressure was measured using a Heise HPO 0-150 psia pressure transducer at pressures above 1.2 kPa. At lower pressures, the pressure was measured with a 10 torr Baratron pressure transducer. The Heise pressure transducer was calibrated by the manufacturer to 0.1 kPa below 200 kPa and 0.5 kPa above 200 kPa. A calibration by comparing readings to a calibrated 1000 torr Baratron was conducted one year after installation. No change in the slope was observed, but a correction due to drift in the zero point was applied to the data. The cause of the drift was assigned to the radiation field as the transducer was within one inch of the container. The standard deviation for pressures below 200 kPa remained at 0.1 kPa with this correction. The 10 torr Baratron transducer (MKS 122 A) and readout were calibrated by the manufacturer to 0.12% of the reading.

A Pfeiffer dry diaphragm vacuum pump (TSH 071 E) was used in all experiments. Gas compositions in the container were measured by gas chromatography (Agilent 6890) on samples withdrawn from the container. These measurements were taken to verify the purity of the gas phase in the powder bed. Sensitivity to impurity gases was 0.001 kPa. The GC was calibrated using calibration gases purchased from Scott Specialty Gases. At low pressures ($P < 0.9$ kPa) with helium as a fill gas, approximately 10% of the gas phase was nitrogen due to outgassing from the powder bed at the higher temperatures. At these conditions, the effective thermal conductivity is relatively insensitive to the gas thermal conductivity because solid–solid conduction and thermal radiation are the dominant heat transfer pathways. Thus, the presence of the nitrogen gas should not significantly affect the results.

The PuO_2 powder was prepared by nitric acid anion exchange followed by oxalate precipitation. The oxalate precipitate was dried and calcined to 873.2 K to produce PuO_2. Four batches of PuO_2 powder produced in this manner were screened and V-blended for 1 h. This powder was calcined to 1248.2 K for 4 h and allowed to cool naturally. A 450 g sample was removed for analytical chemistry and physical properties measurements. The remainder was placed in a convenience can that was placed within an airtight container sealed with a Conflat™ flange until use to limit exposure to airborne contaminants, principally water vapor.

The PuO_2 powder was an extremely fine, homogeneous free-flowing powder with a specific surface area of 1.09 m^2/g (5 point nitrogen BET method; Quantachrome Nova 3000). The powder was 87.81% Pu (estimated precision 0.1%) with approximately 0.1% impurities consisting mainly of nitrate, silicon, uranium, and thorium with tens of ppm levels or less of other elements. The remainder was oxygen yielding a $PuO_{2.06}$ stoichiometry. The measured specific activity was 2.33 ± 0.01 W kg^{-1} Pu (2.05 ± 0.01 W kg^{-1} material). The measured gas pycnometer density was $11.54 \pm 0.03 \times 10^3$ kg m^{-3}. Bulk density of the material within the container was calculated to be $2.54 \pm 0.02 \times 10^3$ kg m^{-3} resulting in a porosity of 0.780 ± 0.008. Relevant experimental parameters used in the model calculations, including PuO_2 mass and bed dimensions, are summarized in Table 1.

Table 1
PuO_2 bed properties

Parameter	Value
ρ_{PuO_2}	11.54×10^3 kg m^{-3}
q_{PuO_2}	2.05 W kg^{-1}
m_b	5.00 kg
ε_b	0.780
R_b	5.7 cm
L_b	19.2 cm

In porous bed heat transfer experiments, it is beneficial to obtain characterization data for the powder, such as particle size and shape, to better estimate particle parameters for effective thermal conductivity models. Unfortunately, due to the radioactive nature of the PuO_2 powder, it is not trivial to obtain accurate characterization data and we do not have these data for the specific powder that was measured in this study. However, particle size data are available from a PuO_2 powder that was processed using the same processes and under similar processing conditions [8]. In that particle size study, Machuron-Mandard and Madic measured the particle size and specific surface area of PuO_2 powders that had been calcined to temperatures between 723.2 and 1323.2 K. The measured specific surface areas for their powder calcined to 1223.2 K and 1323.2 K were 2.1 m^2/g and 1.2 m^2/g. These values are in reasonable agreement with the measured specific surface area of 1.1 m^2/g for the PuO_2 powder calcined to 1248.2 K in our current study. The average particle size measured by Machuron-Mandard and Madic of their PuO_2 powder was approximately 10 μm spherical equivalent diameter, irrespective of calcination temperature. Microscopic images revealed that the particles were irregularly shaped (i.e. non-spherical) which could lead to high porosities such as observed in the current powder. Thus, the best estimate of the mean particle diameter in the PuO_2 powder for this study is approximately 10 μm.

In this study, the effects of pressure and type of fill gas on the thermal behavior of the PuO_2 powder bed were measured. The pressure was varied between 0.055 and 334.4 kPa and helium and argon were used as fill gases. Using helium and argon as fill gases provided a large gas conductivity range because the conductivities of these two gases differ by almost a factor of 10 near ambient pressure. At atmospheric pressure in the continuum regime, helium's thermal conductivity is 0.157 W m^{-1} K^{-1} and argon's thermal conductivity is 0.018 W m^{-1} K^{-1} at 300 K [9]. Initially, the container with the powder was evacuated to remove all residual gases and then filled with either helium or argon until the highest desired pressure was reached. Subsequent measurements at lower pressures were made by removing some of the fill gas and waiting until steady state was established. The time required to reach thermal steady state was approximately 4 h. The resulting radial temperature profile was then recorded from the 10 radial thermocouples in the PuO_2 powder bed.

3. Experimental results

The temperature profile data were primarily used to provide basic information about heat transfer mechanisms in the powder. The effects of pressure and fill gas on the centerline temperature in the PuO_2 powder bed are shown in Fig. 2. The temperature measurements in Fig. 2 have an error of 1.7 K corresponding to the accuracy of the thermocouples. The other contribution of error to the temperature measurements arises from the displacement of the thermocouples from the reported radial position. The error due to the radial displacement of the thermocouples is estimated by comparing the measured radial temperature profiles to calculated parabolic radial profiles for radial heat conduction with constant internal heat generation and uniform effective thermal conductivity. In Fig. 3, the measured radial temperature profiles for the powder with argon are shown along with parabolic fits to the centerline and endpoint temperatures. The x-axis error bars in Fig. 3 are estimated from the average differences in the measured and calculated temperatures for the helium and argon temperature measurements at each radial thermocouple position. From the figure, most of the measured temperatures are in good agreement with the temperatures predicted by the parabolic shape that is expected for this configuration. The largest apparent radial position error is -0.3 cm for the thermocouple at $x = -4.7$ cm. From the calculated temperatures, it appears that this thermocouple is most likely at $x = -5.0$ cm.

The error in the centerline temperatures in Fig. 2 is estimated by assuming that the center thermocouple is also displaced by the maximum 0.3 cm. Since the maximum measured temperature gradient between the middle two thermocouples is 1.7 °/cm, the maximum error in the centerline temperature is 0.5 K. The total error in the absolute centerline temperatures from the thermocouple accuracy error and the radial displacement error is 1.8 K. The

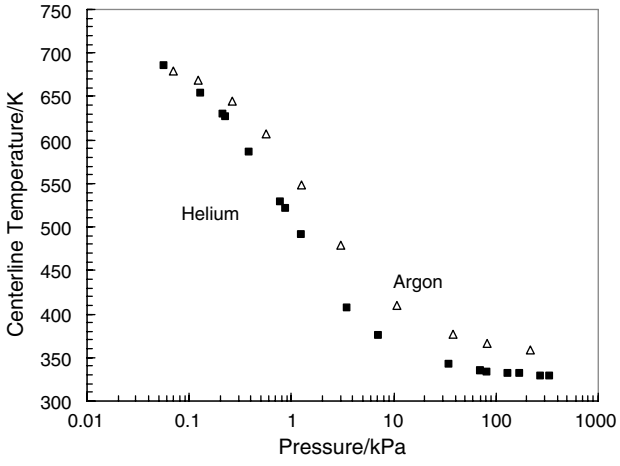

Fig. 2. Measured centerline temperatures for the PuO_2 powder bed with argon and helium as fill gases at different pressures. The average error in these temperatures is 1.8 K.

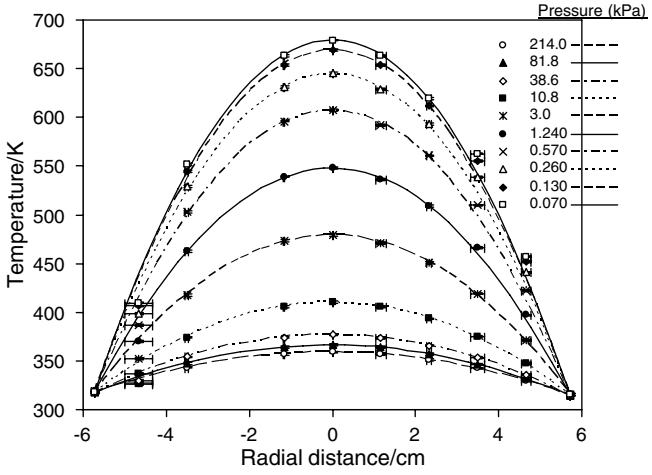

Fig. 3. Radial temperature profiles for PuO_2 powder bed with argon as the fill gas. The points are experimental data and the lines are parabolic fits at each pressure to the centerline and wall temperatures of the bed. The x-axis error bars for each thermocouple are calculated from the average difference between the predicted and measured radial temperature profiles for both argon and helium.

Table 2
Measured radial temperature differences from $r = 0$ to $r = R$ in the PuO_2 bed

Helium		Argon	
P (kPa)	ΔT (K)	P (kPa)	ΔT (K)
334.4	14.4	214.0	43.7
277.6	15.1	81.8	51.7
173.2	16.5	38.6	61.2
130.4	17.7	10.8	94.8
82.2	20.3	3.0	164.1
69.8	21.4	1.240	232.6
35.0	27.4	0.570	291.9
7.0	60.7	0.260	329.9
3.6	92.7	0.130	353.6
1.2	175.7	0.070	364.2
0.890	206.1		
0.770	212.6		
0.390	269.6		
0.225	310.6		
0.210	314.0		
0.130	337.3		
0.055	369.2		

temperature error for changes in temperature, for instance the temperature change for a particular thermocouple when the pressure is changed, is conservatively estimated to be 0.1 K. The standard deviations of the temperature differences between the 10 thermocouples and a reference eleventh thermocouple over 10 days (or 998 readings) ranges from 0.11 K to 0.05 K with an average standard deviation of 0.07 K. Thus, the relative error in the radial temperature differences across the bed is estimated to be 0.1 K, much less than the absolute error of the thermocouple measurement.

The measured radial temperature distributions are used to estimate the effect of the experimental parameters (pressure and fill gas) on the effective thermal conductivity. Assuming that conduction is the dominant heat transfer mechanism, the effective thermal conductivity is inversely proportional to the temperature drop across the bed since heat generation and bed geometry are uniform. The radial temperature drops across the bed are tabulated in Table 2.

The system pressure has a dramatic effect on the effective thermal conductivity, as evidenced by the large increase in radial temperature drop with decreasing pressure in Figs. 2 and 3 and Table 2. At the lowest pressures, the measured temperature drops across the bed are approximately equal for both fill gases as shown in Fig. 2 and Table 2, indicating that the effective thermal conductivities with the different fill gases become independent of fill gas and pressure. At these conditions, the thermal conductivity of the gas becomes unimportant because the dominant heat transfer pathways are thermal radiation and conduction between solid particles.

At higher pressures, the effective thermal conductivity is typically dominated by the gas thermal conductivity. In the plutonium oxide powder, the effective thermal conductivity was expected to differ significantly for the two fill gases because the gas conductivity of helium is approximately eight times that of argon. However, the radial temperature drop with argon as the fill gas was only three times larger than with helium. These results indicate that at higher pressures conduction through the solid particles may be significant since the effective thermal conductivity with argon as the fill gas is higher than expected relative to helium. In many powder beds, the solid does not play a large role in the effective thermal conductivity at high pressures. The role of the solid in the effective thermal conductivity will be further assessed in the modeling section of this paper.

The radial temperature drop increases with decreasing pressure due to the dependence of the effective thermal conductivity on the gas thermal conductivity. Generally, at lower pressures, the gas is in the free molecular regime where the gas thermal conductivity is a linear function of pressure [10]. However, as pressures increase to near ambient, the gas transitions to the continuum regime where the gas thermal conductivity is independent of pressure. From Table 2, the gases do not appear to be in the continuum regime even at pressures above atmospheric pressure in this powder. For example, the temperature drop with helium fill gas decreases from 17.7 K at 130.4 kPa to 14.4 K at 334.4 kPa. If the gases were in the continuum regime, the temperature drop across the bed would be constant across this pressure range. This measured pressure dependence above atmospheric pressure is unexpected and is further explored in the modeling section.

4. Conductivity model development

The packed-bed effective thermal conductivity models from the reviews by Tsotsas and Martin [5], Xu et al. [6], and Kaganer [7] were studied in this work prior to our

model development. The goal was to find a model that would reproduce the pressure dependence of the centerline temperatures in Fig. 2, especially at higher pressures where a pressure dependence exists above atmospheric pressure and the effective thermal conductivity with argon is enhanced relative to that with helium. Unfortunately, no models were able to capture the complex pressure dependence that was measured for the plutonium oxide powder with both fill gases over the large pressure range in this study. Unless they contained many parameters, these models typically predicted higher centerline temperatures than were observed at the higher Ar pressures. Also, many of the models overestimated the centerline temperatures at low pressures with both fill gases where solid–solid conduction and thermal radiation dominate. Both of these results indicate that the models underpredict the effective thermal conductivity of this powder. One reason for the underprediction could be that the solid has a larger role in thermal conduction in this powder than would be assumed for a powder with this high of a porosity. Since the existing models were unable to reproduce the experimental temperature profiles, a new thermal conductivity model was developed for the plutonium oxide powder.

We propose a model that has a similar unit cell to that used by Masamune and Smith [11] and Hayashi et al. [12]. These models contain a unit cell with three parallel pathways through the gas, the solid, and the gas and solid in series. To derive relationships for model parameters, the authors utilized a volumetric unit cell with two contacting hemispheres [11,12]. With these assumptions, the maximum porosity in these models is 0.476, corresponding to loose packing of equal sized spheres. The PuO_2 bed used in the current study has a porosity of 0.780 which is much larger than 0.476 since the particles are very fine and not spherical. The Masamune and Smith or Hayashi et al. model could be used to model heat conduction in the PuO_2 powder if the particles are assumed to be porous spheres with a porosity of 0.568. However, with this additional assumption, a thermal conductivity expression is required for the porous particles. Many porous solids relationships are available in the literature that predict porous particle thermal conductivities over a range of two orders of magnitude and can have varying degrees of dependence on the system pressure [13,14]. It is difficult to choose an appropriate model for the particles in this powder since the nature of these particles is unknown.

Due to the limited information available on particle characterization and packing in the PuO_2 powder [8], we derived a model with no limiting assumptions on porosity or particle shape. This model contains more fit parameters than the previous models [11,12], however it is also applicable to a wider range of powders. The effective thermal conductivity expression was derived from the model in Fig. 4a and the schematic in Fig. 4b. Heat conduction occurs through two parallel pathways in the "gas" and "solid" regions of the powder. The bed porosity (ε_b) is used to define the relative areas of the "gas" and "solid" regions

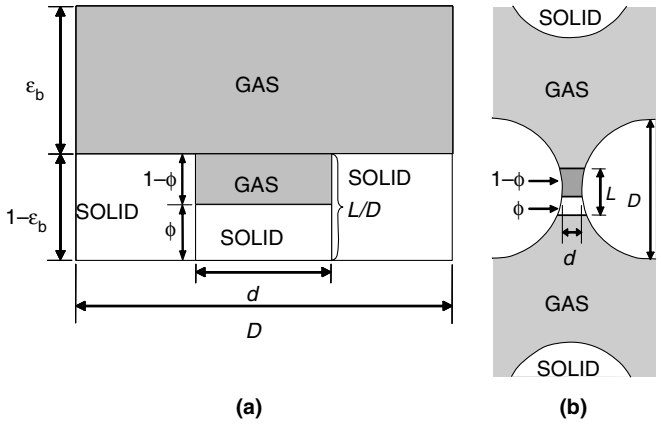

Fig. 4. (a) Model for the effective thermal conductivity expression and (b) idealized schematic of particle packing and contact in the powder.

in the powder. The "gas" region is defined here as the gas-only region of the powder whereas the "solid" region contains two solid particles in series with an interparticle domain that contains both solid–solid and gas–solid conduction pathways. Because the conductances (G) are additive for parallel pathways, the effective thermal conductivity (k_{eff}) is written as

$$k_{eff} = \varepsilon_b k_{g,o} + (1 - \varepsilon_b)(L/D)k_s \tag{1}$$

In Fig. 4a, the "solid" region denoted by the area, $1 - \varepsilon_b$, has the conductivity, k_s. Within the $1 - \varepsilon_b$ region, the interparticle contact fraction (L/D) defines the region where conduction will occur between the solid particles. Multiplying k_s by the factor L/D, as shown in Eq. (1), is a simplification that results from noting that the thermal conductivity of the solid particles (k_{solid}) is large compared with thermal conduction across the gas-filled gap between the particles. Within the interparticle contact region, conduction will occur by both solid–solid contact with area proportional to ϕ (the sphericity parameter) and solid–gas–solid contact with area proportional to $1 - \phi$. The term sphericity is used to define the parameter (ϕ) because it describes the fractional contact between the particles. If the particles were perfect spheres, ϕ would approach zero and if the particles were completely flat, ϕ would approach one.

The unit thermal conductance of the "solid" region (k_s/D), is a series combination of conductance through the solid particles and the interparticle region that can be written as

$$\frac{D}{k_s} = \frac{D - d}{k_{solid}} + \frac{d}{k_{in}} \tag{2}$$

The interparticle region contains parallel gas and solid conductance pathways, so k_{in} has a form similar to Eq. (1) above. With the k_{in} expression, the conductivity of the solid region is as follows:

$$k_s = \left[\frac{\delta}{\phi k_{solid} + (1 - \phi)k_{g,in}} + \frac{(1 - \delta)}{k_{solid}}\right]^{-1} \tag{3}$$

In Eq. (3), the parameter, δ, is the dimensionless contact roughness and is defined as the interparticle distance (d) divided by the total cell distance (D). The gas thermal conductivity in Eq. (3), $k_{g,in}$, is the gas conductivity in the interparticle area where the effective pore size is much smaller than the pore size in the outer "gas" region.

To calculate the effective thermal conductivity from Eqs. (1) and (3), the input parameters or variables are the bed porosity (ε_b), the outer and interparticle gas thermal conductivities ($k_{g,o}$ and $k_{g,in}$), the solid thermal conductivity (k_{solid}), the sphericity (ϕ), the contact roughness (δ), and the interparticle contact fraction (L/D). The bed porosity is experimentally measured (Table 1) and the gas and solid thermal conductivities are available from the literature as discussed below. The sphericity, contact roughness, and interparticle contact fraction are fit parameters obtained from the temperature profile data in this investigation because of limited information on the shape or roughness of the powder particles.

4.1. PuO_2 thermal conductivity

The PuO_2 solid thermal conductivity has been measured in a number of studies [15–17]; however, an expression that correlates these data as a function of temperature is unavailable. Also, the PuO_2 thermal conductivity data from these studies were measured at temperatures above 473 K, but we require solid thermal conductivities at temperatures as low as 323 K. Thus, we needed to develop a reliable expression for the temperature dependence of the thermal conductivity to predict the thermal conductivity at lower temperatures. As part of this study, we reviewed the available PuO_2 thermal conductivity data and developed a temperature dependent correlation using the common relationship for a Debye dielectric solid, where B_1 and B_2 are constants in Eq. (4).

$$k_{solid} = \frac{1}{B_1 + B_2 T} \tag{4}$$

In the PuO_2 thermal conductivity studies [15–17], the thermal diffusivity of PuO_2 was measured and the thermal conductivity determined using the definition

$$k_{solid} = \kappa_T \rho C_p \tag{5}$$

While Fukushima et al. [16] and Gibby [15] used heat capacity values and temperature-dependent densities for PuO_2, Lagedrost et al. [17] estimated the PuO_2 heat capacities from UO_2 values. Since Lagedrost et al. [17] provided their raw diffusivity data and new PuO_2 heat capacity values and densities are available from Carbajo et al. [18], we recalculated the Lagedrost et al. [17] thermal conductivity values to reflect the better known PuO_2 physical property data. The recalculated thermal conductivity values are 1 to 8 % higher than the reported Lagedrost et al. [17] values.

The thermal conductivity data from these studies were corrected because the PuO_2 samples in these studies had theoretical densities between 93% and 96.5%. The conductivity values were corrected to 100% T.D. (theoretical density) using the Maxwell–Eucken equation for low porosity solids.

$$k_{solid} = k_{expt} \frac{1 + \varepsilon_{solid}/2}{1 - \varepsilon_{solid}} \tag{6}$$

In Eq. (6), k_{solid} is the thermal conductivity of 100% T.D. solid, while k_{expt} is the experimentally measured thermal conductivity of the solid with porosity equal to ε_{solid}. With the 100% T.D. conductivity values, the parameters, B_1 and B_2, in Eq. (4) were estimated by linear regression. A comparison of the data and the regressed equation with $B_1 = 1.22 \times 10^{-3}$ m K W^{-1} and $B_2 = 2.75 \times 10^{-4}$ m W^{-1} is shown in Fig. 5. From the figure, Eq. (4) reproduces the thermal conductivity data well over a wide temperature range. In our temperature region of interest between 300 and 700 K, this expression predicts that the solid thermal conductivity changes by a factor of two with a value of 11.9 W m^{-1} K^{-1} at 300 K and 5.2 W m^{-1} K^{-1} at 700 K.

4.2. Gas thermal conductivities

Due to the wide pressure range examined in this study ($P = 0.055$ to 334.4 kPa), the gas thermal conductivity operates in different regimes. At high pressures, the gas thermal conductivity is in the continuum regime where the conductivity is relatively independent of system pressure. Tabulated continuum thermal conductivities for argon and helium were used from the property library in the Engineering Equation Solver (EES) computer program [19,20]. At low pressures, the gas thermal conductivity operates in the free molecular regime where it is a linear function of pressure [10].

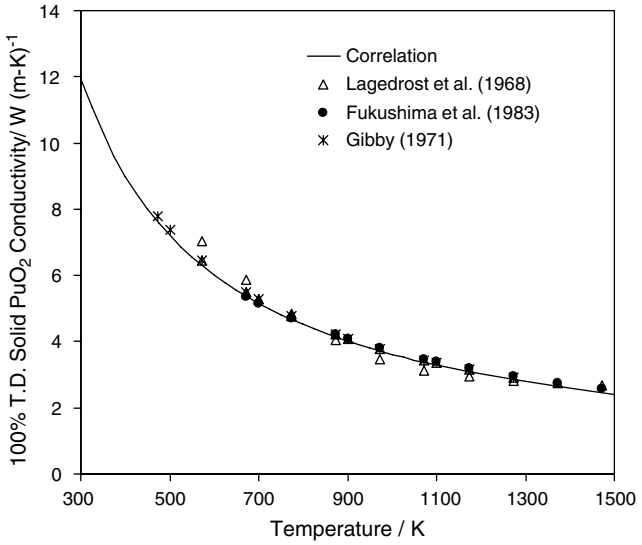

Fig. 5. Comparison of PuO_2 thermal conductivity data and the correlation in Eq. (4) with $B_1 = 1.22 \times 10^{-3}$ m K W^{-1} and $B_2 = 2.75 \times 10^{-4}$ m W^{-1}.

$$k_{\mathrm{fm}} = \left(\frac{\alpha}{2-\alpha}\right)\lambda \Lambda_{\mathrm{o}} P \sqrt{\frac{T_{\mathrm{ref}}}{T}} \tag{7}$$

In Eq. (7), α is the thermal accommodation coefficient, λ is the pore size which is used as the characteristic length in this problem, Λ_{o} is a gas dependent constant tabulated for argon (0.697 W m^{-2} K^{-1} Pa^{-1}) and helium (2.202 W m^{-2} K^{-1} Pa^{-1}), and T_{ref} is the reference temperature (273 K) [10]. Typical values for the thermal accommodation coefficients for argon and helium of 0.9 and 0.5, respectively, are used [21].

At intermediate pressures, a transition region exists where the gas thermal conductivity is a function of both the continuum and free molecular thermal conductivities [21].

$$k_{\mathrm{trans}} = \frac{k_{\mathrm{fm}}}{1 + k_{\mathrm{fm}}/k_{\mathrm{cont}}} \tag{8}$$

The pressure limits of the different operating regimes are determined by the Knudsen number, which is the ratio of the mean free path (l) and the characteristic length scale in the powder, the pore size (λ).

$$Kn = \frac{l}{\lambda} \tag{9}$$

$$l = \frac{k_{\mathrm{B}} T}{\sqrt{2}\pi D_{\mathrm{m}}^2 P} \tag{10}$$

The molecular diameter (D_{m}) is 0.358 nm for Ar and 0.215 nm for He [9]. From Springer [21], the free molecular regime is defined at $Kn > 50$, while the continuum regime is defined at $Kn < 0.01$. At Kn values between 0.01 and 50, the gas thermal conductivity is calculated using Eq. (8). Most pressures in the current experimental pressure range are in the transition region due to the small particle and pore sizes in the PuO_2 powder.

Because we defined two gas thermal conductivities ($k_{\mathrm{g,o}}$ and $k_{\mathrm{g,in}}$) in our model in Eqs. (1) and (3), two appropriate pore sizes in the powder must also be estimated. In the "gas" region in Fig. 4a, the outer pore size is λ_{o} to calculate $k_{\mathrm{g,o}}$ and in the gas-solid area of the "solid" region in Fig. 4a, the interparticle pore size is λ_{in} to calculate $k_{\mathrm{g,in}}$. These pore sizes are not readily known and must be estimated to calculate the gas thermal conductivities and Kn numbers.

5. Temperature profile calculation

The temperature profiles for this system were calculated by finite difference method using the program, Engineering Equation Solver (EES). The solution employed eight radial nodes across the 5.7 cm radius of the PuO_2 powder bed and four axial nodes across half of the powder bed length assuming axial symmetry. The lengths of the axial nodes were chosen such that the temperature at the center of the second axial node is at approximately the same height as the bed thermocouples. Heat transfer pathways were represented by conductances including radial and axial heat transfer through the powder bed ($G_{\mathrm{r},i,j}$ and $G_{\mathrm{ax},i,j}$) and convection from the exterior can wall to the surrounding air (G_{ext}). The expressions for the conductances in the model are as follows:

$$G_{\mathrm{r},i,j} = \frac{2\pi L_j}{\ln(R_{i+1}/R_i)}\left(k_{\mathrm{eff},i,j} + \frac{\sigma(T_{i,j}+T_{i+1,j})(T_{i,j}^2+T_{i+1,j}^2)}{n_{\mathrm{emiss}}(2/e-1)}\right) \tag{11}$$

$$G_{\mathrm{ax},i,j} = \frac{2\pi(R_{i,\mathrm{out}}^2 - R_{i-1,\mathrm{out}}^2)}{\left(\frac{L_j+L_{j+1}}{2}\right)}\left(k_{\mathrm{eff},i,j} + \frac{\sigma(T_{i,j}+T_{i,j+1})(T_{i,j}^2+T_{i,j+1}^2)}{n_{\mathrm{emiss}}(2/e-1)}\right) \tag{12}$$

$$G_{\mathrm{ext}} = h_{\mathrm{ext}} A_{\mathrm{ext}} \tag{13}$$

In the equations above, the index i is for the radial nodes and the index j is for the axial nodes. R_i is the radius at the center of node i, $R_{i,\mathrm{out}}$ is the outer radius of node i, and L_j is the axial length at the center of node j.

The first term in the axial and radial conductances in Eqs. (11) and (12) accounts for thermal conduction and the second term accounts for thermal radiation between nodes. In the radiation term, e is the emissivity, σ is the Stefan–Boltzmann constant, and n_{emiss} is the density of the radiation cells to account for the radiation length scale being much smaller than the node length [7]. For these oxide particles, the emissivity was assumed to be 0.9. The thermal radiation terms in Eqs. (11) and (12) include a temperature dependence so that thermal radiation will have a T^4 dependence in the heat balance equation below. In addition to these thermal conductance pathways, the PuO_2 powder bed provides a heat source with a constant generation rate.

With these conductances, the heat balance for each node was calculated using the following equation:

$$\begin{aligned} &Q_{\mathrm{gen},i,j} + G_{\mathrm{r},i-1,j}(T_{i-1,j} - T_{i,j}) + G_{\mathrm{ax},i,j-1}(T_{i,j-1} - T_{i,j}) \\ &\quad = G_{\mathrm{r},i,j}(T_{i,j} - T_{i+1,j}) + G_{\mathrm{ax},i,j}(T_{i,j} - T_{i,j+1}) \end{aligned} \tag{14}$$

In Eq. (14), $Q_{\mathrm{gen},i,j}$ is the heat generation rate in each node.

Along with Eq. (14) for each node, the model also contains a boundary equation at the bed wall.

$$\begin{aligned} &(G_{\mathrm{r,nrad},j})(T_{\mathrm{nrad},j} - T_{\mathrm{w}}) + \sum_i G_{\mathrm{ax},i,\mathrm{nax}}(T_{i,\mathrm{nax}} - T_{\mathrm{w}}) \\ &\quad = G_{\mathrm{ext}}(T_{\mathrm{w}} - T_{\mathrm{a}}) \end{aligned} \tag{15}$$

The bottom of the bed is assumed to be at the same temperature as the bed wall. Because the thermal conductivity of the stainless steel container is large relative to the powder and the wall thickness is small, the outer temperature of the powder bed is assumed to be the same as the container exterior wall temperature.

To calculate the temperature profiles from Eqs. (14) and (15), the experimental bed parameters in Table 1 (adjusted for half of the bed volume) are employed along with the external heat transfer coefficient, h_{ext}, the external surface area of the bed, A_{ext}, and the air temperature, T_{a}. From the experimental measurements, the air temperature was 301.7 K and the external surface area for half of the bed

was 4.47×10^{-2} m^2. The external heat transfer coefficient, h_{ext}, was 8.45 W m^{-2} K^{-1} as determined from the known total heat generation of half of the bed (5.125 W) and measured wall and air temperatures in the system.

6. Modeling results and discussion

The radial temperature profiles were calculated from Eq. (1) and Eqs. (11)–(15) and the calculated centerline temperatures at a height of 6.0 cm are compared to the measured centerline temperatures as a function of pressure in Fig. 6. To solve these equations, there are several unknown parameters that must be estimated including the interparticle contact fraction (L/D) in Eq. (1), the sphericity (ϕ) and contact roughness (δ) in Eq. (3), the outer and interparticle pore sizes (λ_o and λ_{in}) in Eqs. (7) and (9), and the effective density of the radiation cells (n_{emiss}) in Eqs. (11) and (12). The parameter values that best fit the data are included in Table 3. The fitted parameter values imply that the particles are not perfect spheres ($L/D = 0.086$), have relatively small gaps between the particles ($\delta = 2.86 \times 10^{-3}$), and have few solid–solid contacts in the interparticle contact area ($\phi = 1.71 \times 10^{-4}$). Due to the high porosity of the powder and microscopic images of similar powders, we would expect the particles to be non-spherical and to have point contacts between particles [8]. The interparticle pore size is much smaller than the outer pore size as would be expected from the low estimate of δ and the outer pore size (15.6 μm) is of the order of magnitude estimated for the diameter of plutonium oxide particles [8]. The effective density of the radiation cells ($n_{emiss} = 1.05 \times 10^4$) implies that there is a radiation cell size of 95 μm in this powder (about six times the estimated pore size in this powder).

With the fit parameters in Table 3, the calculated centerline temperatures agree well with the experimental data for both argon and helium across the entire pressure range as shown in Fig. 6. Our effective thermal conductivity expression captures the difference between the fill gases at high pressures where conduction through the solid pathways remains significant in this system. Other effective thermal conductivity models do not account for significant conduction through the solid phase at high pressures and thus are unable to accurately predict the argon centerline temperatures at high pressures in the PuO_2 powder bed. From Table 4 for argon, thermal conduction through the solid pathways accounts for more than 80% of k_{eff} at $P =$ 333 kPa.

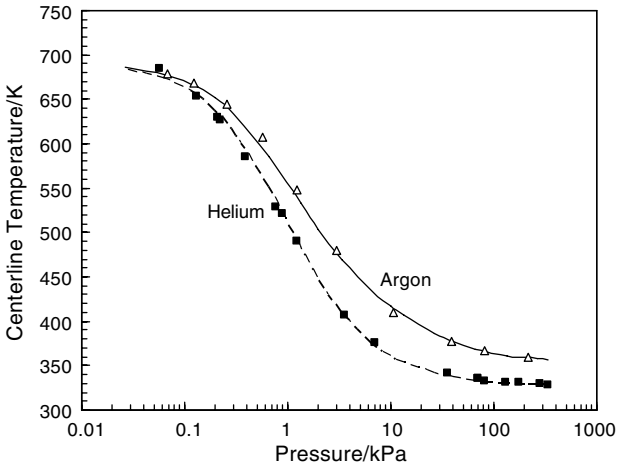

Fig. 6. Comparison of calculated centerline temperatures with experimental data. The dashed line is calculated from the model for helium, the solid line is calculated for argon, and the points are the experimental data. The average error in the experimentally measured temperatures is 1.8 K.

Table 3
Fit parameters for temperature profile calculation

Parameter	Value
δ	2.86×10^{-3}
ϕ	1.71×10^{-4}
L/D	0.086
λ_{in} (μm)	0.56
λ_o (μm)	15.6
n_{emiss}	1.05×10^4

Our effective thermal conductivity expression also captures the low pressure behavior where the helium and argon centerline temperatures approach each other (Fig. 6). From Table 4, the effective thermal conductivities become approximately equal as the pressure decreases. At low pressures, the two primary heat transfer mechanisms are thermal radiation and solid–solid conduction; the thermal conductivity of the gas is unimportant at these conditions. At these pressures, the thermal radiation and conduction terms in Eqs. (11) and (12) are of the same order of magnitude indicating that both pathways are important.

Not only are the centerline temperatures correctly predicted as a function of pressure, but the calculated radial temperature profiles are also in good agreement with the experimental data, as shown in Fig. 7 for the PuO_2 powder with argon as a fill gas. The radial profile calculations are in especially good agreement for the lower pressure data where heat transfer occurs by both thermal radiation and conduction through the powder. The shape of the radial temperature profile could not be correctly predicted at lower pressures unless thermal radiation was included in the model. Because of the large temperature gradient across the bed at these conditions and the temperature dependent thermal radiation term, the bed temperature profile is very sensitive to the bed emissivity. Thus, the correct prediction of the radial temperature profiles at most conditions demonstrates that the contributions of radial conduction and thermal radiation are correctly captured in this model.

The model also captures the experimentally measured pressure dependence at higher pressures for both fill gases. The effective thermal conductivity exhibits a pressure dependence at these higher pressures because the gas conductivity is in the transition regime due to the small pore size (0.56 μm) in the interparticle contact fraction. For example at 333 kPa, the Kn number for helium is 0.12

Table 4
Calculated thermal conductivities for PuO_2 powder at the centerline temperature and a bed height of 6 cm with helium and argon fill gases

P (kPa)	Helium			Argon		
	εk_g	$(1-\varepsilon)(L/D)k_s$	k_{eff}	εk_g	$(1-\varepsilon)(L/D)k_s$	k_{eff}
3.3E+02	1.3E−01	1.5E−01	**2.8E−01**	1.6E−02	7.5E−02	**9.1E−02**
2.7E+02	1.3E−01	1.4E−01	**2.7E−01**	1.6E−02	7.3E−02	**8.9E−02**
2.0E+02	1.3E−01	1.3E−01	**2.6E−01**	1.6E−02	7.0E−02	**8.7E−02**
1.3E+02	1.2E−01	1.2E−01	**2.3E−01**	1.6E−02	6.5E−02	**8.2E−02**
6.7E+01	1.1E−01	8.8E−02	**1.9E−01**	1.6E−02	5.4E−02	**7.0E−02**
4.0E+01	9.4E−02	6.8E−02	**1.6E−01**	1.6E−02	4.4E−02	**6.0E−02**
2.7E+01	8.2E−02	5.3E−02	**1.4E−01**	1.5E−02	3.7E−02	**5.2E−02**
1.3E+01	5.9E−02	3.5E−02	**9.4E−02**	1.4E−02	2.6E−02	**4.0E−02**
1.0E+01	5.0E−02	2.9E−02	**7.9E−02**	1.4E−02	2.2E−02	**3.6E−02**
6.7E+00	3.7E−02	2.3E−02	**6.0E−02**	1.2E−02	1.8E−02	**3.0E−02**
3.3E+00	2.1E−02	1.6E−02	**3.7E−02**	9.3E−03	1.3E−02	**2.2E−02**
2.0E+00	1.3E−02	1.2E−02	**2.5E−02**	6.9E−03	1.0E−02	**1.7E−02**
1.3E+00	8.5E−03	1.0E−02	**1.9E−02**	5.1E−03	9.0E−03	**1.4E−02**
6.7E−01	4.1E−03	8.1E−03	**1.2E−02**	2.8E−03	7.5E−03	**1.0E−02**
2.7E−01	1.6E−03	6.6E−03	**8.2E−03**	1.2E−03	6.4E−03	**7.5E−03**
2.0E−01	1.2E−03	6.4E−03	**7.6E−03**	8.7E−04	6.2E−03	**7.1E−03**
1.3E−01	7.7E−04	6.1E−03	**6.9E−03**	5.8E−04	6.0E−03	**6.6E−03**
6.7E−02	3.8E−04	5.9E−03	**6.2E−03**	2.9E−04	5.8E−03	**6.1E−03**
2.7E−02	1.5E−04	5.7E−03	**5.9E−03**	1.2E−04	5.7E−03	**5.8E−03**

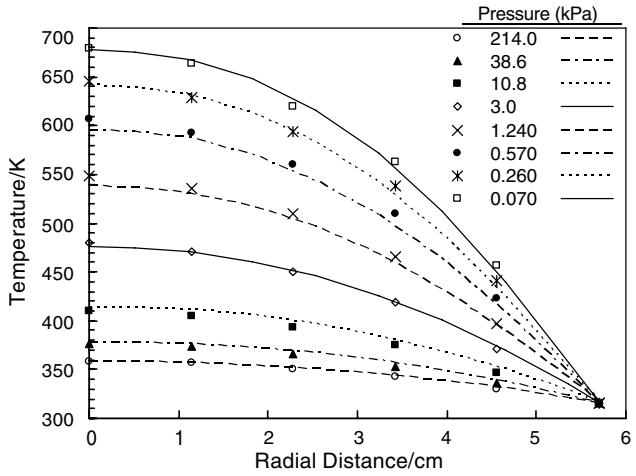

Fig. 7. Calculated and experimental radial temperature profiles with argon as fill gas.

which is in the transition regime. We predict that the thermal conductivity of the powder with helium as the fill gas does not become pressure independent until the pressure reaches approximately 3800 kPa. For the powder with argon present, the transition to the continuum regime occurs at a lower pressure of approximately 1300 kPa due to argon's mean free path being smaller than helium's.

7. Conclusions

The radial temperature profiles of a plutonium dioxide powder bed have been experimentally measured over a pressure range of 0.055–334.4 kPa with two different fill gases, argon and helium. From these measurements, the effective thermal conductivities of the powder with argon or helium as fill gas at low pressures are approximately equal because the dominant heat transfer mechanisms are thermal radiation between particles and solid–solid conduction. At high pressures, the differences between the effective thermal conductivities with helium and argon as the fill gas are smaller than expected, indicating that conduction through the solid is significant even at the highest pressures in these powders. Also, the effective thermal conductivity has a pressure dependence at near ambient pressures, even though gas thermal conductivities are typically assumed to be in the continuum regime and independent of pressure at these conditions.

Because the PuO_2 powders examined in this study are very fine particles with random shapes and high porosity, most existing effective thermal conductivity models are unsuitable due to limiting assumptions about particle packing or size. The effective thermal conductivity expression presented herein was derived assuming conduction pathways that exist in parallel and in series in the powder. With the proposed effective thermal conductivity expression, the temperature profiles were accurately predicted over the entire experimental pressure range for two very different fill gases. The pressure dependence at high pressures exists due to a small interparticle pore size (0.56 μm) in the fine powder. In these powders, thermal conduction through the solid region enhanced by free molecular effects plays a larger role than is typically found in most packed beds. Due to its generality, this model is suitable for other fine ceramic powders that have high porosities and unknown particle shapes, sizes, and packing geometry.

Acknowledgements

We acknowledge the following people at Los Alamos National Laboratory for their help in conducting the experiments and collecting the data (John Berg, Dennis

Padilla, Max Martinez, Alex Carrillo, Laura Worl, David Harradine, and Thad Knight). We would like to thank the reviewers for their insightful comments, which have resulted in a more focused and hopefully clearer presentation of our results. Funding for this investigation was provided by the Surveillance and Monitoring Program, United States Department of Energy Office of Environmental Management and conducted at Los Alamos National Laboratory operated by the University of California for the US Department of Energy under contract W-7405-ENG-36.

References

[1] Stabilization, Packaging, and Storage of Plutonium-Bearing Materials, DOE−STD-3013-2000, U.S. Department of Energy, Washington, DC, 2000.
[2] T.D. Knight, R.G. Steinke, Thermal analysis of plutonium materials in British Nuclear Fuels, Ltd., containers, Los Alamos National Laboratory Report, LA-UR-97-1866, 1997.
[3] S. Hensel, Thermal analysis of the 9975 package as a plutonium storage container, Westinghouse Savannah River Company Report, WSRC-TR-98-00203, 1998.
[4] R.G. Deissler, C.S. Eian, Investigation of effective thermal conductivities of powders, National Advisory Committee for Aeronautics report, NACA-RM E52C05, 1952.
[5] E. Tsotsas, H. Martin, Thermal conductivity of packed beds: a review, Chem. Eng. Progress 22 (1987) 19–37.
[6] M. Xu, M.A. Abdou, A.R. Raffray, Thermal conductivity of a beryllium gas packed bed, Fus. Eng. Des. 27 (1995) 240–246.
[7] M.G. Kaganer, Thermal Insulation in Cryogenic Engineering, IPST Press, Jerusalem, 1969.
[8] X. Machuron-Mandard, C. Madic, Plutonium dioxide particle properties as a function of calcination temperature, J. Alloys Compds. 235 (1996) 216–224.
[9] D.R. Lide (Ed.), CRC Handbook of Chemistry and Physics, 84th ed., CRC Press, 2003.
[10] J.M. Lafferty (Ed.), Foundations of Vacuum Science and Technology, John Wiley & Sons, New York, 1998.
[11] S. Masamune, J.M. Smith, Thermal conductivity of beds of spherical particles, Ind. Eng. Chem. Fundam. 2 (2) (1963) 136–143.
[12] S. Hayashi, K. Kubota, H. Masaki, Y. Shibata, K. Takahashi, A theoretical model for the estimation of the effective thermal conductivity of a packed bed of fine particles, Chem. Eng. J. 35 (1) (1987) 51–60.
[13] J.B. Butt, Thermal conductivity of porous catalysts, AIChE J. 11 (1) (1965) 106–112.
[14] T. Akiyama, H. Ohta, R. Takahashi, Y. Waseda, J. Yagi, Measurement and modeling of thermal conductivity for dense iron oxide and porous iron ore agglomerates in stepwise reduction, ISIJ Int. 32 (7) (1992) 829–837.
[15] R.L. Gibby, The effect of plutonium content on the thermal conductivity of (U,Pu)O_2 solid solutions, J. Nucl. Mater. 38 (1971) 163–177.
[16] S. Fukushima, T. Ohmichi, A. Maeda, M. Handa, Thermal conductivity of $(Pu_{1-x}Nd_x)O_{2-y}$ and $(Pu_{1-x}Y_x)O_{2-y}$ solid solutions, J. Nucl. Mater. 115 (1983) 118–127.
[17] J.F. Lagedrost, D.F. Askey, V.W. Storhok, J.E. Gates, Thermal conductivity of PuO_2 as determined from thermal diffusivity measurements, Nucl. Appl. 4 (1968) 54–61.
[18] J.J. Carbajo, G.L. Yoder, S.G. Popov, V.K. Ivanov, A review of the thermophysical properties of MO_x and UO_2 fuels, J. Nucl. Mater. 299 (3) (2001) 181–198.
[19] B.A. Younglove, H.J.M. Hanley, The viscosity and thermal conductivity coefficients of gaseous and liquid argon, J. Phys. Chem. Ref. Data 15 (4) (1986) 1323–1327.
[20] R.D. McCarty, V.D. Arp, A new wide range equation of state for helium, Adv. Cryog. Eng. 35 (1990) 1465–1475.
[21] G.S. Springer, Heat transfer in rarefied gases, in: T.F. Irvine, J.P. Hartnett (Eds.), Advances in Heat Transfer, vol. 7, Academic Press, New York, 1971, pp. 163–218.